Ga-substitution-induced single ferroelectric phase in multiferroic $CuFeO_2$

N. Terada,[1,2,3] T. Nakajima,[4] S. Mitsuda,[4] H. Kitazawa,[2] K. Kaneko,[3] and N. Metoki[3]
[1]*ICYS, National Institute for Materials Science, Namiki 1-1, Tsukuba, Ibaraki 305-0044, Japan*
[2]*Neutron Scattering Group, National Institute for Materials Science, Sengen 1-2-1, Tsukuba, Ibaraki 305-0047, Japan*
[3]*Japan Atomic Energy Agency, 2-4 Shirakata Shirane, Tokai, Naka, Ibaraki 319-1195, Japan*
[4]*Department of Physics, Faculty of Science, Tokyo University of Science, Tokyo 162-8601, Japan*
(Received 31 March 2008; revised manuscript received 10 June 2008; published 3 July 2008)

We have succeeded in realizing a single ferroelectric phase in $CuFe_{0.963}Ga_{0.037}O_2$ by substituting nonmagnetic Ga^{3+} for Fe^{3+} sites in $CuFeO_2$. Ferroelectric polarization P in $CuFe_{0.963}Ga_{0.037}O_2$ is observed below 7.5 K, and has the relatively large value of $\sim 250\ \mu C/m^2$, which is comparable to $P=300\sim 400\ \mu C/m^2$ in the magnetic-field-induced ferroelectric phase of $CuFeO_2$. In neutron-diffraction measurements, a single magnetic diffraction peak with an incommensurate wave number was observed below 7.5 K in $CuFe_{0.963}Ga_{0.037}O_2$, indicating that the ferroelectric-incommensurate (FEIC) phase is realized as a single phase. Therefore, $CuFe_{0.963}Ga_{0.037}O_2$ with a single FEIC phase is strongly expected to provide the best opportunity to investigate unresolved problems regarding the ferroelectric mechanism in $CuFeO_2$. In this paper, we report measurements of magnetic susceptibility, specific heat, pyroelectric, dielectric constant, and neutron diffraction of a single crystal of $CuFe_{0.963}Ga_{0.037}O_2$.

DOI: 10.1103/PhysRevB.78.014101 PACS number(s): 77.80.−e, 75.80.+q, 75.50.Ee, 75.25.+z

I. INTRODUCTION

Since the discovery of the magnetic-field-induced ferroelectric phase transition in $CuFeO_2$ (Ref. 1), the magnetoelectric coupling in this compound has attracted considerable attention. Unlike the well-studied magnetoferroelectrics induced by cycloidal-type helical magnetic orderings such as $TbMnO_3$ (Refs. 2 and 3) and $CoCr_2O_4$ (Ref. 4), the proper helical magnetic structure induces ferroelectric polarization in $CuFeO_2$ (Refs. 5–8). According to recently developed theories,[9] there are three coupling mechanisms between the spin and electric-dipole moment in multiferroics. The first one is the exchange striction mechanism in which the electric-dipole moment $\boldsymbol{p}$ is proportional to $\boldsymbol{S}_i \cdot \boldsymbol{S}_j$. The second is based on spin current theory,[10] which derives the relation between $\boldsymbol{p}$, spin, and the vector connecting the two spin sites $\boldsymbol{e}_{ij}$ as $\boldsymbol{p} \propto \boldsymbol{e}_{ij} \times (\boldsymbol{S}_i \times \boldsymbol{S}_j)$. In almost all multiferroics with spiral magnetic orderings, the ferroelectricity is explained in terms of the second mechanism.[11] In $CuFeO_2$, on the other hand, the magnetic structure in the ferroelectric-incommensurate (FEIC) phase is a proper helical one whose screw axis is parallel to the propagation vector, i.e., $\boldsymbol{S}_i \times \boldsymbol{S}_j \| \boldsymbol{e}_{ij}$ (Ref. 5). The appearance of electric polarization in the FEIC phase, therefore, cannot be explained by the second mechanism. The third mechanism originates from the combined effect of *d-p* hybridization and spin-orbit coupling. A recent theoretical study[7] has argued that the ferroelectricity in $CuFeO_2$ is caused by the third mechanism. However, currently, no experimental studies have been reported that confirm this theory.

The magnetic properties of $CuFeO_2$ have been extensively studied over the past 15 years (Refs. 12–15). $CuFeO_2$ has a delafossite structure, which belongs to the space group $R\bar{3}m$ at room temperature [see Fig. 1(a)]. At low temperature, two-step magnetic phase transitions occur at $T_{N1}=14$ K and $T_{N2}=11$ K (Ref. 13). In $T_{N2} \leq T \leq T_{N1}$, a partially disordered (PD) phase is realized where the collinear magnetic moments are approximately aligned with the hexagonal c axis and are sinusoidally modulated along the [110] axis with the incommensurate wave vector $(q\ q\ \frac{3}{2})$ (Refs. 13 and 16). Below T_{N2}, a four-sublattice (4SL) magnetic structure with collinear magnetic moments along the c axis is realized where the wave vector is the commensurate $(\frac{1}{4}\frac{1}{4}\frac{3}{2})$. Recent x-ray diffraction studies have revealed that the magnetic orderings are realized with the help of the lattice distortion to lift the degeneracy in the exchange energy.[17–19]

The effect of nonmagnetic substitution on magnetic properties has been extensively studied for $CuFe_{1-x}Al_xO_2$ (Refs. 5, 16, and 20–22). Kanetsuki *et al.*[23] and Seki *et al.*[24] have discovered nonmagnetic substitution-induced ferroelectricity in the FEIC phase in zero magnetic field. Terada *et al.*[22] obtained the x-T magnetic phase diagram of $CuFe_{1-x}Al_xO_2$ up to $x=0.04$ [see Fig. 1(b)], which consists of four magnetic phases: 4SL, PD, FEIC, and oblique PD (OPD) phases. The magnetic ground state of the 4SL phase varies with x in the FEIC phase with the proper helical magnetic structure[5] and ferroelectricity[23,24] for $0.014 \leq x \leq 0.035$. In the FEIC phase, magnetic Bragg reflections are observed at $(q\ q\ \frac{3}{2})$ and $(\frac{1}{2}\ -q\ \frac{1}{2}\ -q\ \frac{3}{2})$ with $q \sim 0.207$ in the previous neutron-diffraction measurements.[22] In $x \geq 0.035$, the collinear magnetic structure with oblique moments are realized in the OPD phase where the propagation wave vector is $(q\ q\ \frac{3}{2})$ with $q \sim 0.196$ (Refs. 16 and 22).

Nakajima *et al.*[5] have demonstrated that the FEIC phase of $CuFe_{1-x}Al_xO_2$ coexists with the intermediate PD phase by performing neutron-diffraction measurements with applied magnetic fields. They also discovered that the single FEIC phase without coexistence with the intermediate PD phase can be obtained by cooling under a magnetic field of 4 T. The single FEIC phase of pure $CuFeO_2$ is realized above 7 T. The application of strong magnetic fields is thus necessary to obtain the single FEIC phase in both $CuFeO_2$ and $CuFe_{1-x}Al_xO_2$. Experimental setups are restricted by a superconducting magnet applying strong magnetic fields; prevent-

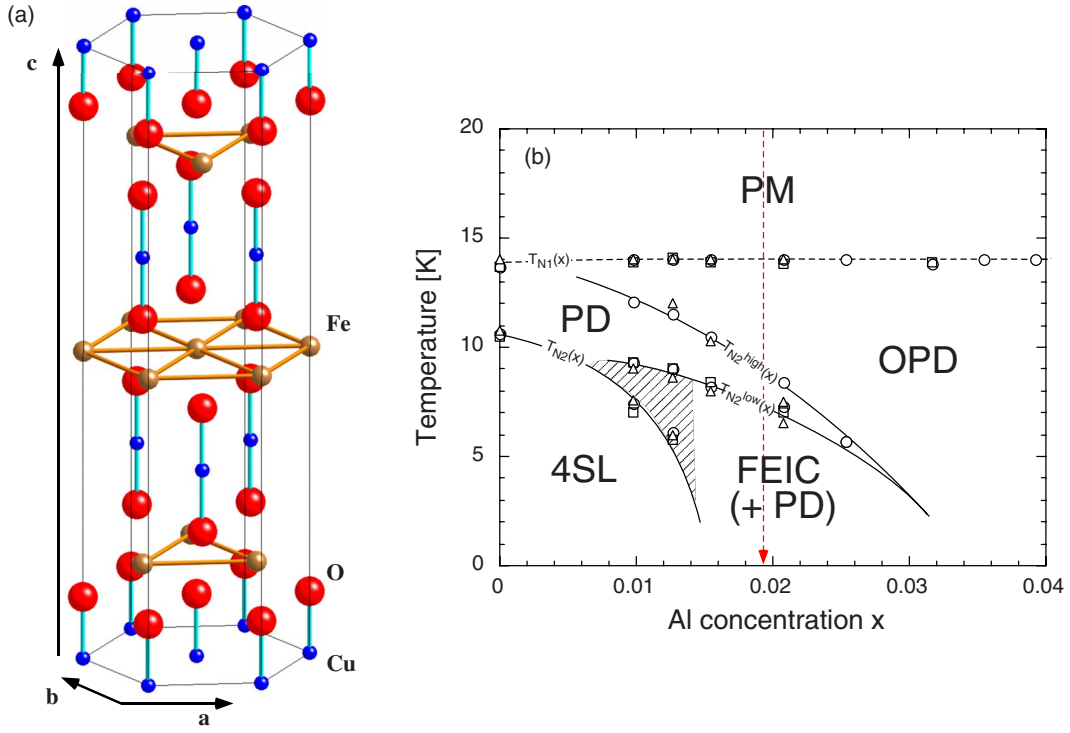

FIG. 1. (Color online) (a) Crystal structure of $CuFeO_2$. (b) x-T magnetic phase diagram of $CuFe_{1-x}Al_xO_2$. The data were taken from Ref. 22. The phase-transition temperatures in the Al concentration are denoted by the dotted line with the arrow corresponds to those in $CuFe_{1-y}Ga_yO_2$ with $y=0.037$ (see the main text for details).

ing us from investigating the microscopic mechanism of ferroelectricity in detail. A sample in which the FEIC phase is realized without the coexistence of the PD phase in a zero magnetic field is strongly required for further investigation.

To realize the single FEIC phase, we consider the two kinds of effect of the nonmagnetic substitution on the exchange paths when the nonmagnetic ions are substituted for magnetic ions. One is simply cutting the exchange paths around the nonmagnetic site. The other is local lattice distortion around the nonmagnetic site, which is caused by the difference in the ionic radius between magnetic Fe^{3+} and the nonmagnetic ion. We anticipate that the latter effect is comparatively large because of the big difference in the ionic radii of Al^{3+} and Fe^{3+}, and that this might cause the coexistence of the PD phase. On this basis, we selected Ga^{3+}, which has an ionic radius close to that of Fe^{3+} as the nonmagnetic impurity. In this paper, we report measurements of magnetic susceptibility, specific heat, pyroelectric, dielectric constant, and neutron-diffraction spectra of a single crystal of $CuFe_{1-y}Ga_yO_2$ with $y=0.037$.

II. EXPERIMENTAL DETAILS

A single crystal of $CuFe_{1-y}Ga_yO_2$ with $y=0.037$ was grown by the floating-zone technique.[25] The Ga concentration was determined by inductively coupled plasma-optical emission spectrometry (ICP-OES). ICP-OES, which is a multielement analysis method, was used in this study since the analyzed sample had a mass of ~400 mg. For the magnetic-susceptibility measurements, we used the magnetic property measurement system of quantum design (QD). For specific-heat measurements, we used the QD's physical property measurement system. For pyroelectric measurements, we used an electrometer (Keithley, 6517A). The dielectric constant was measured at 10 and 100 kHz using an *LCR* meter. The neutron-diffraction measurements were carried out with the cold neutron triple-axis spectrometers HER and LTAS installed at the guide hall of JRR-3 in Tokai. A single crystal, which had a mass of 483 mg, was mounted with the $[1\bar{1}0]$ axis vertical in a He-pumped cryostat for HER and closed-cycle He-gas refrigerator for LTAS, so as to provide access to the (HHL) scattering plane. The incident neutron wave numbers are 1.55 $Å^{-1}$ for HER and 1.30 $Å^{-1}$ for LTAS. We used a Be filter for HER to suppress contamination by higher orders.

III. RESULTS

A. Temperature dependence of bulk properties

The temperature dependence of the magnetic susceptibility parallel $\chi_{\parallel}(T)$ and perpendicular $\chi_{\perp}(T)$ to the c axis are shown in Fig. 2(a). At 14 K, a small peak anomaly appears in $\chi_{\parallel}(T)$ and $\chi_{\perp}(T)$. While isotropic behavior was observed in $T \geq 10$ K during cooling and in $T \geq 11$ K during heating, anisotropic behavior appears below 10 K on cooling and below 11 K on heating. A large thermal hysteresis was observed in $\chi_{\parallel}(T)$ in 7.1 K $\leq T \leq 11$ K. At 7.1 K on cooling and 7.5 K on heating, discontinuous reductions were observed in both $\chi_{\parallel}(T)$ and $\chi_{\perp}(T)$. These anomalies observed in the susceptibility of $CuFe_{0.963}Ga_{0.037}O_2$ are quite similar to

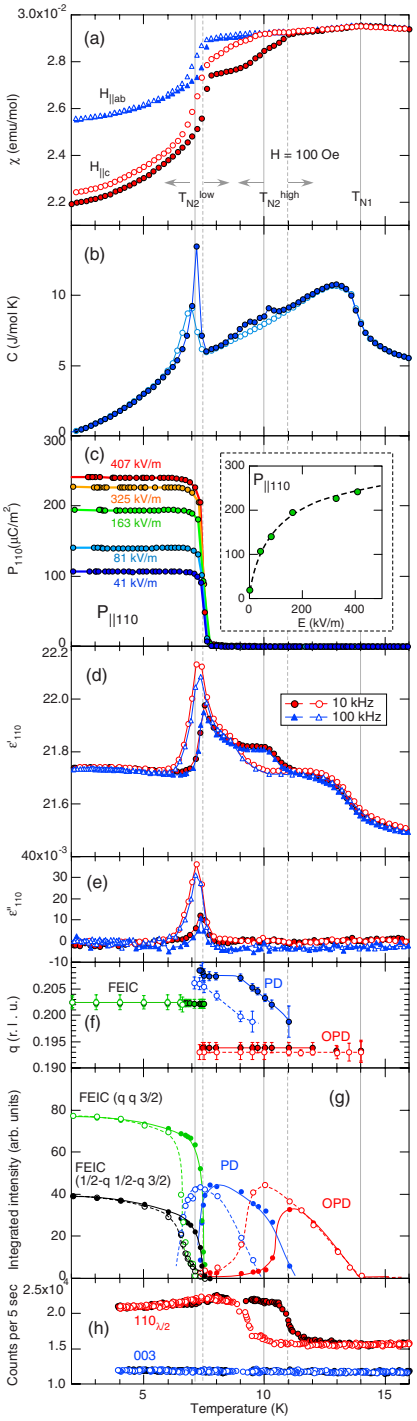

FIG. 2. (Color online) Temperature dependence of (a) magnetic susceptibility χ (b) specific heat C (c) electric polarization P_{110} (d) real part of dielectric constant ε'_{100} (e) imaginary part of dielectric constant along the [110] axis ε''_{110} (f) propagation wave number q of magnetic modulations (g) integrated intensity of the magnetic Bragg reflections and (h) peak intensity of the nuclear Bragg reflections at $(110)_{\lambda/2}$ (Ref. 27) and (003). Open and closed symbols denote the data for decreasing and increasing temperature processes, respectively. (c) P_{110} was measured after cooling with several poling electric fields of 407, 325, 163, 81, and 41 kV/m. The inset in (c) shows the poling electric-field dependence of P_{110} at 2 K. Solid and dotted lines denote the magnetic phase-transition temperatures for cooling and warming processes, respectively.

those in $CuFe_{1-x}Al_xO_2$ (Ref. 22). Therefore, in accordance with the previously reported definitions for the phase-transition temperatures in $CuFe_{1-x}Al_xO_2$ (Ref. 22), we define three transition temperatures during cooling for $CuFe_{1-y}Ga_yO_2$ as $T_{N1}=14$ K [from paramagnetic (PM) to OPD], $T_{N2}^{\text{high}}=10$ K (from OPD to PD) and $T_{N2}^{\text{low}}=7.1$ K (from PD to FEIC).

In the temperature dependence of the specific heat $C(T)$ the gradient of $C(T)$ changes at T_{N1} as shown in Fig. 2(b). Thermal hysteresis was observed in $C(T)$ for 8.5 K$\leq T \leq$11 K. The temperature region in which the hysteresis was observed in $C(T)$ is different from that in $\chi_{\|}(T)$. No significant anomaly appears in $C(T)$ at T_{N2}^{high}. On the other hand, a sharp peak anomaly appears at T_{N2}^{low}.

As shown in Fig. 2(c), electric polarization P_{110} appears below T_{N2}^{low}. The inset shows the electric-field dependence of P_{110} during heating. The maximum value of P_{110} is about 250 μC/m^2, which is comparable to the value 300 $\sim$400 μC/m^2 observed in $CuFeO_2$ (Ref. 1). The real part of the dielectric constant $\varepsilon'_{110}(T)$ and the imaginary part of the dielectric constant along the 110 axis $\varepsilon''_{110}(T)$ show significant anomalies as shown in Figs. 2(d) and 2(e). The gradient of $\varepsilon'_{110}(T)$ changes at T_{N1} and T_{N2}^{high}. $\varepsilon'_{110}(T)$ also exhibits thermal hysteresis for 8.5 K$\leq T \leq$11 K, which is coincident with that in $C(T)$, not that in $\chi_{\|}(T)$. At T_{N2}^{low}, a peak anomaly appears in both the $\varepsilon'_{110}(T)$ and $\varepsilon''_{110}(T)$ during cooling and heating.

B. Neutron-diffraction measurements

Typical neutron-diffraction profiles in $CuFe_{0.963}Ga_{0.037}O_2$ are shown in Fig. 3(b). The reciprocal (HHL) zone is schematically illustrated in Fig. 3(a). In the OPD phase, the magnetic Bragg reflection is observed at (0.194 0.194 $\frac{3}{2}$) in the reciprocal-lattice space in which the wave number is independent of temperature [see Fig. 2(f)]. In the PD phase, this reflection is observed at (q q $\frac{3}{2}$) with temperature dependent q [see Figs. 2(f) and 2(g)]. The linewidth is much broader than the experimental resolution. These results are in good agreement with those for $CuFe_{0.98}Al_{0.02}O_2$ (Ref. 21).

On the other hand, there is a relatively sharp enhancement in the reflections characteristic of the FEIC phase, (q q $\frac{3}{2}$) and ($\frac{1}{2}-q$ $\frac{1}{2}-q$ $\frac{3}{2}$) with $q=0.202$ below T_{N2}^{low} as shown in Figs. 2(g) and 3. The wave number differs slightly from $q=0.207$ in the FEIC phase of $CuFe_{1-x}Al_xO_2$ (Ref. 22) within the experimental accuracy. In $CuFe_{1-x}Al_xO_2$ with $x=0.0155$ (Ref. 22), the contribution of the PD phase remains below T_{N2}^{low} (see the inset of Fig. 3). We should note that the incorrect magnetic structure in the FEIC phase was determined in a previous paper owing to the coexistence.[26] In $CuFe_{0.963}Ga_{0.037}O_2$, on the other hand, the contribution of the PD phase is not observed below T_{N2}^{low}. The observed scattering profiles are, however, slightly asymmetric, which might be caused by a slight concentration distribution of the Ga impurity. Note that the difference in the linewidth between the reflections (q q $\frac{1}{2}$) and ($\frac{1}{2}-q$ $\frac{1}{2}-q$ $\frac{3}{2}$) is caused by the difference in the experimental resolution that varies with $\mathbf{Q}$. Taking account of the disappearance of the reflection corresponding to the PD phase below T_{N2}^{low}, we conclude that the

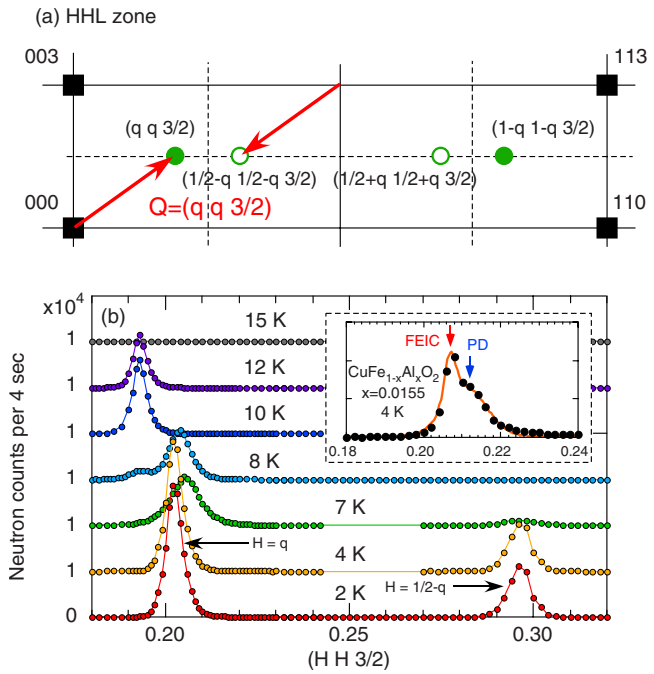

FIG. 3. (Color online) (a) Schematic of the reciprocal (HHL) zone. Squares and circles denote the reciprocal-lattice positions of the nuclear and magnetic reflections, respectively. (b) Typical neutron-diffraction profiles along $(HH\frac{3}{2})$ at several temperatures in $CuFe_{0.963}Ga_{0.037}O_2$. The inset shows the diffraction profiles at 4 K for $CuFe_{1-x}Al_xO_2$ with $x=0.0155$, which was taken from Ref. 22.

single FEIC phase is realized without the coexistence of the PD phase below T_{N2}^{low} in $CuFe_{0.937}Ga_{0.037}O_2$.

As mentioned in the introduction, the 4SL magnetic structure is realized with the lattice distortion to lift the huge degeneracy in the frustrated exchange interactions as has been reported in previous x-ray diffraction studies on $CuFeO_2$ (Refs. 17–19). Although lattice distortion also occurs in the magnetic-field-induced FEIC phase of $CuFeO_2$ (Refs. 18 and 19), no x-ray diffraction study in the FEIC phase of diluted sample has been reported. As shown in Fig. 2(h), the nuclear reflection at $(110)_{\lambda/2}$ (Ref. 27) is enhanced below T_{N2}^{high}, while the reflection at (003) remains unchanged. The enhancement originates from the partial release of the extinction effect, which is caused by the change in the crystal mosaic in the triangular lattice plane due to the monoclinic distortion. This phenomenon has previously been observed in $CuFeO_2$ (Ref. 13) and $CuFe_{1-x}Al_xO_2$ (Refs. 20 and 21). A large thermal hysteresis in the temperature dependence of $(110)_{\lambda/2}$ (Ref. 27) was observed in 8.5 $\mathrm{K} \leq T \leq 11$ K, which coincides with the temperature region where $C(T)$ and ε'_{110} show the hysteresis [see Figs. 2(b) and 2(d)].

As shown in Figs. 4(b) and 4(c), the linewidth in the reciprocal-lattice scan profile along ($HH0$) around $(110)_{\lambda/2}$ becomes broader below T_{N2}^{high}. The reciprocal-lattice ($HK0$) plane, which shows the separation of the Bragg reflections for the monoclinic distortion is schematically illustrated in Fig. 4(a). The 110 reflection splits into three reflections with two different d values when monoclinic distortion occurs. In $\theta-2\theta$ scan [the ($HH0$) scan indicated by the arrow in Fig. 4(a)], peak separation or broadening should be experimentally observed below the transition temperature. The broadening of the $(110)_{\lambda/2}$ reflection, therefore, indicates a structural phase transition from rhombohedral to monoclinic symmetry below T_{N2}^{high}, which is in good agreement with the x-ray diffraction data in $CuFeO_2$ (Refs. 17–19). We thus find that monoclinic distortion occurs in the PD and the FEIC phases even in $CuFe_{1-y}Ga_yO_2$.

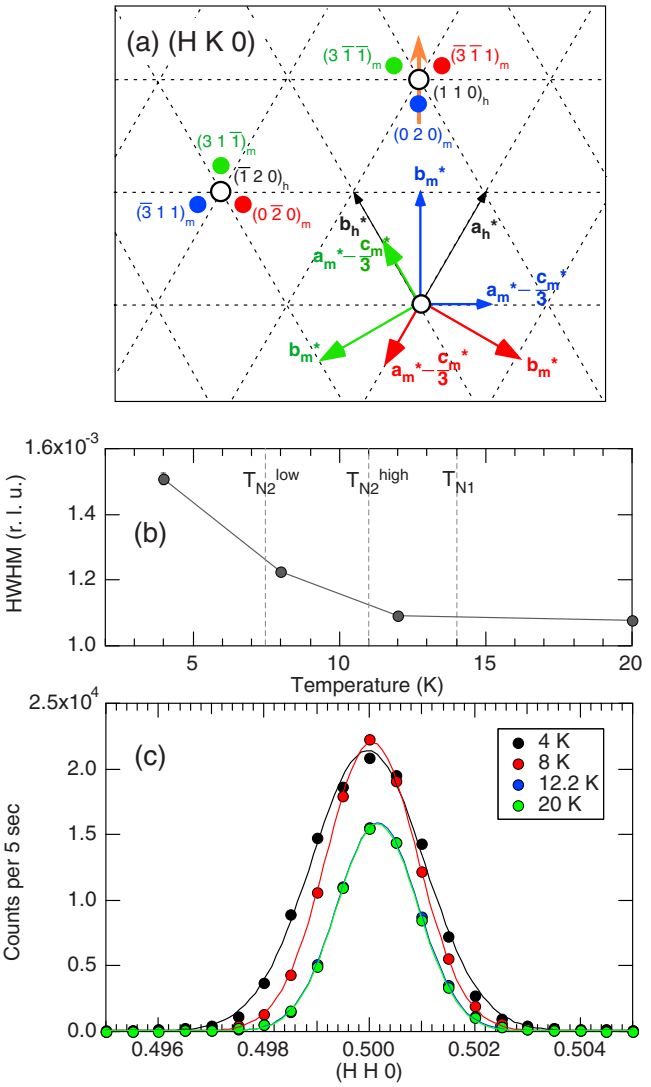

FIG. 4. (Color online) (a) The reciprocal-lattice (HK0) plane. Open and closed circles denote the reciprocal-lattice points for the rhombohedral structure and the distorted monoclinic structure, respectively. The subscripts h and m denote the unit vectors with hexagonal and monoclinic notations [see Fig. 1(b) in Ref. 8], respectively. The arrow on $(110)_h$ denotes the direction of the reciprocal-lattice scan in (c). (b) Temperature dependence of half width at half maximum of the nuclear scattering peak for the ($HH0$) scan around $(110)_{\lambda/2}$. (c) Typical diffraction profiles at $(110)_{\lambda/2}$ at several temperatures.

IV. DISCUSSION

The phase-transition temperatures in $CuFe_{0.963}Ga_{0.037}O_2$ are almost the same as those in $CuFe_{0.98}Al_{0.02}O_2$ (Refs. 22

and 24) as indicated by the dotted line with the arrow in Fig. 1(b). In other words, the nonmagnetic substitution effect of Ga^{3+} is much weaker than that of Al^{3+}. We thus find that the local lattice distortion caused by the difference in the ionic radii between the nonmagnetic ion Ga^{3+} or Al^{3+} and magnetic Fe^{3+} significantly affects the spin states in $CuFeO_2$. Moreover, the local lattice distortion strongly affects whether the PD phase remains at the lowest temperature or not. We here present one possibility to explain the significant difference in the survival of the PD phase between Al and Ga substitutions. In recent x-ray diffraction study on $CuFe_{0.9845}Al_{0.0155}O_2$, Nakajima *et al.*[28] have reported the temperature dependence of the monoclinic lattice constants. The monoclinic lattice constant b contracts discontinuously at T_{N2}^{low} (from FEIC to PD phases) with increasing temperature, which means that b favored in the PD phase for the magnetoelatic energy is smaller than that in the FEIC phase. Note that b is strongly correlated with the magnetic states rather than a, which has been revealed in the previous works.[29,30] When site distances between Fe or Al sites are locally locked into small value around Al ions by the substitution of Al, this local lattice contraction should favor the PD state in the local region around Al ions even below T_{N2}^{low}. Therefore, the PD state might be prevented from disappearing due to the local contraction in $CuFe_{1-x}Al_xO_2$. On the other hand, because of no local lattice contraction in $CuFe_{1-y}Ga_yO_2$, the PD phase should disappear smoothly; as the result, the FEIC phase can be realized as a single phase below T_{N2}^{low}.

There is a significant difference in the phase transition from the PD phase to the FEIC phase at T_{N2}^{low} between $CuFe_{0.963}Ga_{0.037}O_2$ and $CuFe_{1-x}Al_xO_2$. In a previous report for $CuFe_{1-x}Al_xO_2$, it was suggested that the phase transition is second order, because a latent heat was not observed within the experimental accuracy of the specific-heat measurements.[22] However, in the present $CuFe_{0.963}Ga_{0.037}O_2$ data, we observed a latent heat through a deviation of the relaxation curve from the exponential one. We thus conclude that the phase transition from the PD phase to the FEIC phase is first order; the latent heat in $CuFe_{1-x}Al_xO_2$ could not be observed, which is caused by the transition being obscured by the Al concentration distribution.

As mentioned in Sec. I, $CuFeO_2$ is a unique example of multiferroics in which ferroelectricity is induced by proper helical magnetic ordering. In the present study, the single FEIC phase was obtained by substituting nonmagnetic Ga^{3+} making it possible to investigate the microscopic mechanism of the appearance of the ferroelectricity using $CuFe_{1-y}Ga_yO_2$. As an example, we show the relationship between the magnetic order parameter of the proper helical magnetic state and the electric polarization. Comparison of the temperature dependence of P_{110} and the integrated intensity of the magnetic Bragg reflection at $(q\ q\ \frac{3}{2})$ is shown in Fig. 5. As can be clearly seen in this figure, the temperature dependence differs between the two quantities in the FEIC phase. P_{110} does not change at all below 7 K, while the $(q\ q\ \frac{3}{2})$ intensity continues to increase down to 2 K. The experimental results indicate that P_{110} does not correspond to just the magnetic order parameter for the FEIC phase. If P_{110} had any dependence on the magnetic order parameter, then it would change at least slightly in magnitude below 7 K. The experimental results, therefore, suggest that another factor besides a magnetic one is responsible for the variation in the electric polarization. In a recent theoretical study,[7] it has been argued that the ferroelectricity in $CuFeO_2$ and $CuFe_{1-x}Al_xO_2$ originates from Fe $3d$-O $2p$ hybridization and spin-orbit coupling. This theory reveals that the ferroelectricity arises from the term proportional to $\cos 2\theta$, where θ is the angle between the Fe spin and the direction connecting Fe^{3+} and O^{2-}. If the angle θ changes in temperature in the FEIC phase, which is caused by a crystal lattice deformation, the ferroelectricity might depend on the crystal change as well as the magnetic order parameter. In order to gain a deeper understanding of the temperature dependence of P_{110}, an x-ray diffraction study is required to investigate the lattice deformation in detail.

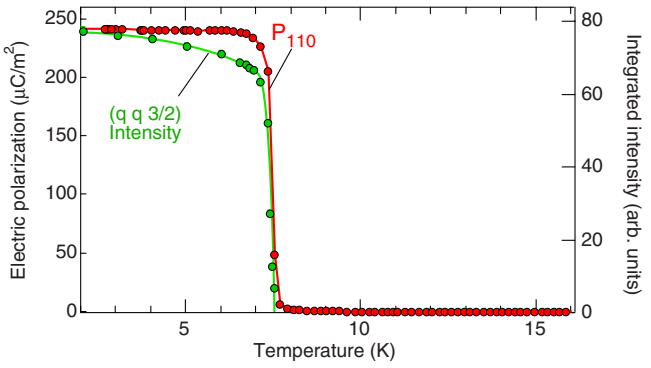

FIG. 5. (Color online) Comparison of the temperature dependence of the electric polarization along the [110] axis $P_{110}(T)$ and the integrated intensity of the magnetic Bragg reflection at $(q\ q\ \frac{3}{2})$.

V. CONCLUSION

We have performed the magnetic susceptibility, specific heat, pyroelectric, dielectric constant, and neutron-diffraction measurements of a $CuFe_{0.963}Ga_{0.037}O_2$ single crystal. The influence of Ga^{3+} impurity on the physical properties of $CuFeO_2$ is much smaller than that of Al^{3+}. Considering that the ionic radius of Ga^{3+} is close to that of Fe^{3+}, we find that the difference in the ionic radii between nonmagnetic ions and magnetic Fe^{3+} resulting in local lattice distortion around the nonmagnetic ion sites, as well as the cutting of the exchange paths, play important roles in the nonmagnetic substitution effect in $CuFeO_2$.

The bulk properties and the microscopic magnetic orderings in the OPD and the PD phases in $CuFe_{0.963}Ga_{0.037}O_2$ are almost the same as those in $CuFe_{1-x}Al_xO_2$. In the FEIC phase of $CuFe_{0.963}Ga_{0.037}O_2$, P is comparatively large with a value $\sim 250\ \mu C/m^2$, which is comparable to $P=300 \sim 400\ \mu C/m^2$ in $CuFeO_2$. In the neutron-diffraction measurements, in contrast to $CuFe_{1-x}Al_xO_2$, a single peak is observed in the FEIC phase of $CuFe_{0.963}Ga_{0.037}O_2$, indicating that the single FEIC phase is realized below 7.5 K without coexistence with the PD phase.

Since $CuFeO_2$ is a unique example of multiferroics in which the ferroelectricity is induced by the proper helical

magnetic ordering, clarification of the mechanism is strongly required. A recent theoretical study has argued that the ferroelectricity in $CuFeO_2$ is caused by the combined effect of *d-p* hybridization and spin-orbit coupling.[7] However, no experimental studies demonstrating this recent theory have been published so far. Therefore, $CuFe_{0.963}Ga_{0.037}O_2$ with the single FEIC phase is strongly expected to provide the best opportunity to study the unresolved problems regarding the ferroelectric mechanism in $CuFeO_2$.

ACKNOWLEDGMENTS

The neutron-diffraction experiments at JRR-3 were partially supported by ISSP of the University of Tokyo [Grant No. 7596B (HER)] and were performed under the Common-Use Facility Program of JAEA. This work was partially supported by Grants-in-Aid for Scientific Research "Young Scientists (B)", Grant No. 20740209 and "Scientific Research (C)", Grant No. 19540377 from the Japan Society for the Promotion of Science.

[1] T. Kimura, J. C. Lashley, and A. P. Ramirez, Phys. Rev. B **73**, 220401(R) (2006).
[2] M. Kenzelmann, A. B. Harris, S. Jonas, C. Broholm, J. Schefer, S. B. Kim, C. L. Zhang, S.-W. Cheong, O. P. Vajk, and J. W. Lynn, Phys. Rev. Lett. **95**, 087206 (2005).
[3] T. Arima, A. Tokunaga, T. Goto, H. Kimura, Y. Noda, and Y. Tokura, Phys. Rev. Lett. **96**, 097202 (2006).
[4] Y. Yamasaki, S. Miyasaka, Y. Kaneko, J.-P. He, T. Arima, and Y. Tokura, Phys. Rev. Lett. **96**, 207204 (2006).
[5] T. Nakajima, S. Mitsuda, S. Kanetsuki, K. Prokes, A. Podlesnyak, H. Kimura, and Y. Noda, J. Phys. Soc. Jpn. **76**, 043709 (2007).
[6] T. Nakajima, S. Mitsuda, S. Kanetsuki, K. Tanaka, K. Fujii, N. Terada, M. Soda, M. Matsuura, and K. Hirota, Phys. Rev. B **77**, 052401 (2008).
[7] T. Arima, J. Phys. Soc. Jpn. **76**, 073702 (2007).
[8] N. Terada, S. Mitsuda, Y. Tanaka, Y. Tabata, K. Katsumata, and A. Kikkawa, J. Phys. Soc. Jpn. **77**, 054701 (2008).
[9] C. Jia, S. Onoda, N. Nagaosa, and J. H. Han, Phys. Rev. B **76**, 144424 (2007).
[10] H. Katsura, N. Nagaosa, and A. V. Balatsky, Phys. Rev. Lett. **95**, 057205 (2005).
[11] S. W. Cheong and M. Mostovoy, Nat. Mater. **6**, 13 (2007).
[12] S. Mitsuda, H. Yoshizawa, N. Yaguchi, and M. Mekata, J. Phys. Soc. Jpn. **60**, 1885 (1991).
[13] S. Mitsuda, N. Kasahara, T. Uno, and M. Mase, J. Phys. Soc. Jpn. **67**, 4026 (1998).
[14] S. Mitsuda, M. Mase, K. Prokes, H. Kitazawa, and H. A. Katori, J. Phys. Soc. Jpn. **69**, 3513 (2000).
[15] O. A. Petrenko, G. Balakrishnan, M. R. Lees, D. M. Paul, and A. Hoser, Phys. Rev. B **62**, 8983 (2000).
[16] N. Terada, T. Kawasaki, S. Mitsuda, H. Kimura, and Y. Noda, J. Phys. Soc. Jpn. **74**, 1561 (2005).
[17] N. Terada, S. Mitsuda, H. Ohsumi, and K. Tajima, J. Phys. Soc. Jpn. **75**, 023602 (2006).
[18] F. Ye, Y. Ren, Q. Huang, J. A. Fernandez-Baca, P. Dai, J. W. Lynn, and T. Kimura, Phys. Rev. B **73**, 220404(R) (2006).
[19] N. Terada, Y. Tanaka, Y. Tabata, K. Katsumata, A. Kikkawa, and S. Mitsuda, J. Phys. Soc. Jpn. **75**, 113702 (2006); N. Terada, Y. Tanaka, Y. Tabata, K. Katsumata, A. Kikkawa, and S. Mitsuda, *ibid.* **76**, 068001 (2007).
[20] N. Terada, S. Mitsuda, S. Suzuki, M. Fukuda, T. Kawasaki, T. Nagao, and H. A. Katori, J. Phys. Soc. Jpn. **73**, 1442 (2004).
[21] N. Terada, S. Mitsuda, K. Prokes, O. Suzuki, H. Kitazawa, and H. A. Katori, Phys. Rev. B **70**, 174412 (2004).
[22] N. Terada, S. Mitsuda, T. Fujii, K. Soejima, I. Doi, H. A. Katori, and Y. Noda, J. Phys. Soc. Jpn. **74**, 2604 (2005).
[23] S. Kanetsuki, S. Mitsuda, T. Nakajima, D. Anazawa, H. A. Katori, and K. Prokes, J. Phys.: Condens. Matter **19**, 145244 (2007).
[24] S. Seki, Y. Yamasaki, Y. Shiomi, S. Iguchi, Y. Onose, and Y. Tokura, Phys. Rev. B **75**, 100403(R) (2007).
[25] T. R. Zhao, M. Hasegawa, and H. Takei, J. Cryst. Growth **166**, 408 (1996).
[26] N. Terada, S. Mitsuda, and A. Gukasov, Phys. Rev. B **73**, 014419 (2006).
[27] The nuclear reflection at (1 1 0) where the length of scattering vector $|Q| \sim 4$ Å was not accessible in this neutron experiment, because $|Q| > 2k_i$. Instead of the inaccessible 110 reflection, we measured the reflection at $(\frac{1}{2}\frac{1}{2}0)$ with half length of scattering vector of the 110 reflection using the second-order higher harmonics of monochromator. $(\frac{1}{2}\frac{1}{2}0)$ is referred to as $(110)_{\lambda/2}$ in this paper.
[28] T. Nakajima, S. Mitsuda, T. Inami, N. Terada, H. Ohsumi, K. Prokes, and A. Podlesnyak, arXiv:0806.2004 (unpublished).
[29] N. Terada, Y. Narumi, K. Katsumata, T. Yamamoto, U. Staub, K. Kindo, M. Hagiwara, Y. Tanaka, A. Kikkawa, H. Toyokawa, T. Fukui, R. Kanmuri, T. Ishikawa, and H. Kitamura, Phys. Rev. B **74**, 180404(R) (2006).
[30] N. Terada, Y. Narumi, Y. Sawai, K. Katsumata, U. Staub, Y. Tanaka, A. Kikkawa, T. Fukui, K. Kindo, T. Yamamoto, R. Kanmuri, M. Hagiwara, H. Toyokawa, T. Ishikawa, and H. Kitamura, Phys. Rev. B **75**, 224411 (2007).